

Theoretical insight into structural and mechanical features of $\text{Hf}_{0.5}\text{Ta}_{0.5}\text{C}$

Jelena Zagorac^{1,2,*}, Dejan Zagorac^{1,2}, Tamara Škundrić^{1,2}, Milan Pejić^{1,2}, Branko Matović^{1,2}, Johann Christian Schön³

¹*Institute of Nuclear Sciences Vinča, Materials Science Laboratory, Belgrade University, Belgrade, Serbia*

²*Center for synthesis, processing, and characterization of materials for application in extreme conditions - CextremeLab, Institute of Nuclear Sciences Vinča, Belgrade, Serbia*

³*Max Planck Institute for Solid State Research, Heisenbergstrasse 1, 70569 Stuttgart, Germany*

Received 5 June 2025; received in revised form 22 June 2025; accepted 28 June 2025

Abstract

Tantalum carbide (TaC) and hafnium carbide (HfC), as well as mixed hafnium tantalum carbides, are of great recent scientific and industrial interest due to their structural features, and thermal, elastic and mechanical properties. In order to identify the possible crystal structure candidates in the $\text{Hf}_{0.5}\text{Ta}_{0.5}\text{C}$ system that are (meta)stable for different pressures, a global search was performed on the energy landscape of the system. The obtained structure candidates were further locally optimized on the DFT level and the relaxed structures were crystallographically analysed and compared. As a result, the experimentally observed rock salt phase was found as a global minimum and dozen additional feasible modifications of $\text{Hf}_{0.5}\text{Ta}_{0.5}\text{C}$ were predicted. Besides the experimentally observed NaCl-type structure, various distorted versions of this structure type were found, as well as modifications exhibiting the NiAs-, ortho- and 5-5-type of structure. Furthermore, mechanical properties including bulk, shear, Young's moduli, elastic constants and the Vicker hardness were computed for all promising predicted structure candidates. We believe that the present results will help in understanding the structure-property relationship in mixed HfC/TaC systems.

Keywords: tantalum hafnium carbide, HfC/TaC, DFT, mechanical properties

I. Introduction

Tantalum and hafnium carbides are classified as ultrahigh-temperature ceramics (UHTCs) due to their high melting points (~3900 °C) which are among the highest for inorganic materials [1,2]. Also, experimental and theoretical investigations have reported the excellent elastic and mechanical properties of HfC and TaC, making them suitable to be employed as structural materials in different applications [3,4], e.g. as thermal protection materials for the next generation of hypersonic vehicles. The reason for the excellent elastic and mechanical properties and extremely high melting temperatures lies in the combination of strong ionic and covalent bonds.

HfC and TaC exhibit the same rock-salt structure type as the thermodynamically stable modification at standard pressure, same as their mixtures form a solid

solution with the general formula $\text{Hf}_x\text{Ta}_{1-x}\text{C}$ over the entire composition range above 887 °C [5]. TaC-HfC composites or solid solutions (at least partially) are usually synthesized by using hot pressing, pressureless sintering, and spark plasma sintering [6,7]. According to Shannon [8] the atomic radii of Hf (0.71 Å) and Ta (0.68 Å) are quite similar, which suggests that Hf and Ta can replace one another in the compounds without changing the initial structure. Furthermore, according to the literature their solid solutions exhibit even better properties, for example, higher melting temperature [9], good mechanical properties, thermal conductivity and thermal stability [10]. Also, since TaC displays a higher degree of plasticity than HfC, adding a small amount of Ta into HfC could improve its plasticity and shear modulus and decrease the coefficient of thermal expansion [11–13]. The powder synthesis reported in the literature is performed mostly on a Ta-rich composition $\text{Hf}_{0.2}\text{Ta}_{0.8}\text{C}$ [14]. In comparison with other members of the $\text{Hf}_x\text{Ta}_{1-x}\text{C}$ system, the $\text{Hf}_{0.5}\text{Ta}_{0.5}\text{C}$ compound, which is the focus of our investigation,

*Corresponding author: tel: + 381 64 1594700
e-mail: jelena@vin.bg.ac.rs

exhibits a higher microhardness (36.71 ± 1.21 GPa), higher elastic modulus (559.30 ± 6.50 GPa), lower oxidation rate and better ablation resistance [15–17]. Furthermore, the solid solutions of the mixed hafnium tantalum carbides show better oxidation resistances than the pure carbides. The best oxidation resistance was observed also in the $\text{Hf}_{0.5}\text{Ta}_{0.5}\text{C}$ composition [7]. The research indicates that balancing the ratio of Ta and Hf is crucial for achieving optimal mechanical properties and oxidation resistance in practical applications. According to the first-principles calculations, the mechanical properties of $\text{Hf}_x\text{Ta}_{1-x}\text{C}$ ($x = 0.2, 0.4, 0.5$) improve as the Ta content increases due to the enhanced bonding between Ta and C atoms [18]. According to literature data [6], the mechanical properties of the solid solution samples exceeded those of the individual HfC and TaC carbides. The exceptional damage tolerance and improved mechanical properties of $\text{Ta}_{0.5}\text{Hf}_{0.5}\text{C}$, compared to other solid solution $\text{Hf}_x\text{Ta}_{1-x}\text{C}$ compositions, make it an extraordinary structural material for hypersonic applications [19]. Previous theoretical works [20,21] revealed that among the five instances of suggested solid solution compounds (i.e. HfC, $\text{Hf}_{0.75}\text{Ta}_{0.25}\text{C}$, $\text{Hf}_{0.5}\text{Ta}_{0.5}\text{C}$, $\text{Hf}_{0.25}\text{Ta}_{0.75}\text{C}$ and TaC), the $\text{Hf}_{0.25}\text{Ta}_{0.75}\text{C}$ solid solution should possess the largest elastic modulus and shear modulus.

II. Computational methods and background

2.1. Determination of feasible structure candidates

From a theoretical point of view, feasible modifications of a chemical system are associated with individual local minima or structurally related groups of such minima, on the energy landscape of the system [22]. In order to identify the local minima of the potential energy in the $\text{Hf}_{0.5}\text{Ta}_{0.5}\text{C}$ system, we started our study with a crystal structure prediction using a global search (GS) method. The global search was performed for six different values of the pressure up to extremely high values of 1600 GPa (0, 0.16, 1.6, 16, 160 and 1600 GPa). The global search procedure implemented in the G42+code [23] was based on the stochastic simulated annealing method combined with many periodic local optimizations along the search trajectories. The moveclass for the random walk included shifts in randomly selected atoms only (65%), exchange of randomly chosen pairs of atoms (10%), and changes in the cell parameters with and without atom movements (25%). To perform the global searches with a reasonable computational effort we used four formula units, and a fast computable empirical two-body potential consisting of the Lennard-Jones and exponentially damped Coulomb terms. Using the LOAD script [24] the resulting large set of candidates is sorted, where their symmetries were determined using the SFND [25] and RGS [26]

algorithms implemented in the program KPLOT [27] and duplicate candidates were eliminated via the CMPZ algorithm [28] implemented in KPLOT.

Besides the GS candidates, we generated feasible candidate structures by starting from some of the lowest energy structure candidates obtained from our previous structure prediction studies for HfC and TaC [29,30]. Here, we constructed new candidates by randomly replacing half of the Hf (Ta) atoms with Ta (Hf) atoms in the earlier low-energy HfC (TaC) modifications.

As a final step, the structure candidates were locally minimized on an *ab initio* level. The symmetries of these optimized structures were again determined using the program KPLOT [27] and the Vesta code [31] was employed for the visualization of the structures.

2.2. Details of the *ab initio* calculations

The CRYSTAL17 code [32,33], which is based on linear combinations of atomic orbitals, was used for the local optimization of the most promising structure candidates on the *ab initio* level. DFT calculations were performed using two different functionals: the local density approximation (LDA) with the Perdew-Zunger (PZ) correlation functional [34] and the generalized gradient approximation (GGA) with the Perdew-Burke-Ernzerhof (PBE) functional [35]. Previous studies have shown that the choice of these DFT functionals produces reliable structure prediction results [29,30,36]. For the integration over the Brillouin zone, a k -point mesh of $8 \times 8 \times 8$ was generated using the Monkhorst-Pack scheme, and the energy convergence tolerance was set as 10^{-7} eV/atom.

Regarding the basis sets, in the case of hafnium a Hf_ECP_Stevens_411d31G_munoz_2007 effective core pseudopotential was employed [37,38] and a Ta_ECP60MDF-31(51df)G_baranek_2013_CsTaO₃ effective core pseudopotential was used for tantalum [39,40]. In the case of carbon, the C_6-21G*_catti_1993 all-electron basis set based on Gaussian-type orbitals was used [40,41].

2.3. Mechanical and elastic properties

The bulk modulus B characterizes the response of a material to the change in the applied pressure Δp ($= p - 0 = p$ in the linear regime) in terms of the change in relative volume $\Delta V/V$: $B = -\Delta p / (\Delta V/V)$. Analogously, the shear modulus G describes the relation between the shear strain γ in the material and the applied external shear stress τ : $G = \tau / \gamma$ [42]. Another mesoscopic quantity of interest for practical applications is the hardness H_V ; it is related to the elastic and plastic properties of materials and can be calculated from the bulk modulus (B) and the shear modulus (K) on a phenomenological level according to following equation [43]:

$$H_V = 0.92(K/B)^{1.137} K^{0.708} \quad (1)$$

In addition, the elastic constants C_{ij} (in the Voigt notation, i.e. $i, j = 1, \dots, 6$) were computed. The elastic constants of a compound describe its response to an applied stress or, the stress needed to maintain a given deformation. Here, we note that the number of independent elastic constants depends on the space group symmetries of the crystalline modification under consideration. Furthermore, the mechanical stability of any crystal requires the strain energy to be positive based on the Born-Huang criteria [44]. As a consequence, we need to fulfil several necessary and sufficient conditions for elastic stability, which vary depending on the crystal system to which the structure candidate belongs [45]. Thus, in the hexagonal and tetragonal case four conditions need to be obeyed:

$$C_{11} > |C_{12}|; \quad 2C_{13}^2 < C_{33}(C_{11} + C_{12}); \quad C_{44} > 0; \quad C_{66} > 0$$

The analogous criteria for an orthorhombic system are:

$$C_{11} > 0; \quad C_{11}C_{22} > C_{12}^2; \\ C_{11}C_{22}C_{33} + 2C_{12}C_{13}C_{23} - C_{11}C_{23}^2 - C_{22}C_{13}^2 - C_3 \\ C_{44} > 0; \quad C_{55} > 0; \quad C_{66} > 0$$

and for the trigonal (rhombohedral) crystals, there are 6 independent elastic constants, $C_{11}, C_{12}, C_{13}, C_{14}, C_{33}, C_{44}$, and the mechanical stability conditions take the following form:

$$C_{11} > |C_{12}|; \quad C_{44} > 0; \quad (C_{11} + C_{12})C_{33} > 2C_{12}^2; \\ (C_{11} - C_{12})C_{44} > 2C_{14}^2$$

Finally, for crystals belonging to the monoclinic systems, 13 independent elastic constants ($C_{11}, C_{12}, C_{13}, C_{15}, C_{22}, C_{23}, C_{25}, C_{33}, C_{35}, C_{44}, C_{46}, C_{55}$ and C_{66}) need to be computed [46]. The monoclinic phases are mechanically stable if their elastic constants C_{ij} meet the following inequalities [47]:

$$C_{ii} > 0 \quad i = 1 - 6; \quad C_{22} + C_{33} > 2C_{23} \\ C_{11} + C_{22} + C_{33} > 2(C_{12} + C_{13} + C_{23}); \\ C_{33}C_{55} > C_{35}^2; \quad C_{44}C_{66} > C_{46}^2; \\ C_{22}C_{33}C_{55} + 2C_{23}C_{25}C_{35} > C_{22}C_{35}^2 + C_{55}C_{23}^2 + C_3 \\ ; \\ 2[C_{15}C_{25}(C_{33}C_{12} - C_{13}C_{23}) + C_{15}C_{35}(C_{22}C_{13} - C_1 \\ C_{25}C_{35}(C_{11}C_{23} - C_{12}C_{13})] > C_{15}^2(C_{22}C_{33} - C_{23}^2) + \\ C_{25}^2(C_{11}C_{33} - C_{13}^2) + C_{35}^2(C_{11}C_{22} - C_{12}^2) + pC_{55}$$

where:

$$p = C_{11}C_{22}C_{33} - C_{11}C_{23}^2 - C_{22}C_{13}^2 - C_{33}C_{12}^2 + 2$$

To calculate these mechanical and elastic properties, the computational strategy implemented in the

CRYSTAL17 solid-state quantum-chemical program [48] was employed. The full elastic tensor was generated using the keyword ELASTCON [49]. Furthermore, in order to evaluate these properties not only for each individual structure candidate but also for a solid solution phase of $\text{Hf}_{0.5}\text{Ta}_{0.5}\text{C}$, we have used the KOVIN algorithm [50] that allows us to deal with the partial occupancies (implied in the averaged structure description of a solid solution) in the calculations in a suitable approximate fashion.

III. Results and discussion

3.1. Structural features

The global search generated almost 30,000 candidate structures, which were found in 68 different space groups (besides $P1$). Most of the candidates exhibiting high degrees of symmetry were obtained at low and moderate pressures, while at extreme pressures of 1600 GPa, most candidates were found only in symmetry $P1$, with often highly distorted coordination polyhedra; this suggests a tendency towards amorphization caused by too much compression and shortening of the bond lengths at such extreme conditions.

After the local optimization, the GS candidates were ranked according to their energy on the *ab initio* level, and the energy/volume curves were computed for the nine structure candidates with the lowest energies. Here we should emphasize that all of these nine candidates (RS1 - RS9, labelled by energy rank) exhibit a more or less distorted rock-salt structure type ranging in symmetry from $R-3m$ (no.166) to $P1$ (no. 2). Thus, not only the global minimum but also many structurally related low-energy local minima belong to this structure prototype both on the empirical potential energy landscape and the *ab initio* energy landscape of $\text{Hf}_{0.5}\text{Ta}_{0.5}\text{C}$. We note that the maximal energy difference among the nine rock salt prototype minima is below 0.02 eV/atom (c.f. Table S1 in the supporting information) and thus we expect the system to form a solid solution phase, at least at intermediary temperatures down to room temperature. This is supported by the observation that the total energy for the Hf/Ta arrangement with the lowest energy in the rock salt prototype structure, i.e. the RS1 structure candidate, $E_h(\text{Hf}_{0.5}\text{Ta}_{0.5}\text{C}) = -90.9646$ Ha, is lower than the sum of the energies of HfC and TaC, $1/2((E_h(\text{HfC}) + E_h(\text{TaC})) = -90.9587$ Ha, indicating that the mixed hafnium tantalum carbide is stable against decomposition into the end members HfC and TaC.

The curves shown in Fig. 1a are obtained using the LDA functional, while the curves in Fig. 1b were obtained using the GGA functional. They show the same ranking of these nine structure candidates. The orthorhombic candidate (RS1) in the $Cccm$ space group is the structure with the lowest total energy (Fig.

2a) and it is followed by the monoclinic $P2$ (RS2) structure in Fig. 2b and the tetragonal $P4_2/mmc$ (RS3) structure (Fig. 2c). Among the best-nine candidates in

the total energy there are three further tetragonal candidates; RS7 (Fig. 2g), RS8 (Fig. 2h) and RS9 (Fig.

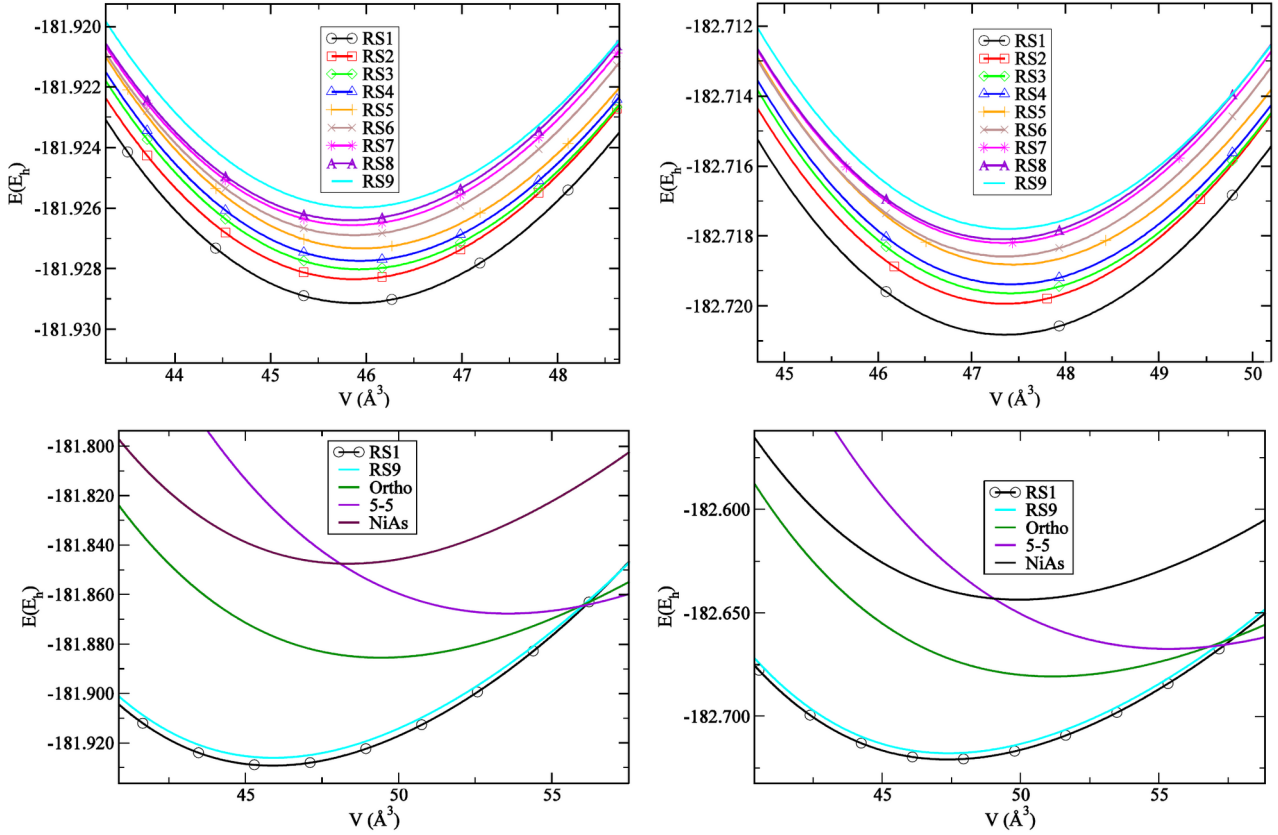


Figure 1. $E(V)$ curves for the nine rock-salt prototype candidates computed using LDA (a) and GGA (b) functionals and for the three other promising modifications (the NiAs proto-type, the ortho prototype and the 5-5 proto-type) using LDA (c) and GGA (d) functionals. For comparison, the $E(V)$ curves for the rock salt type candidates RS1 and RS9 are also shown in (c) and (d). The energy (in units of Hartree) and the volume refer to one formula unit HfTaC_2

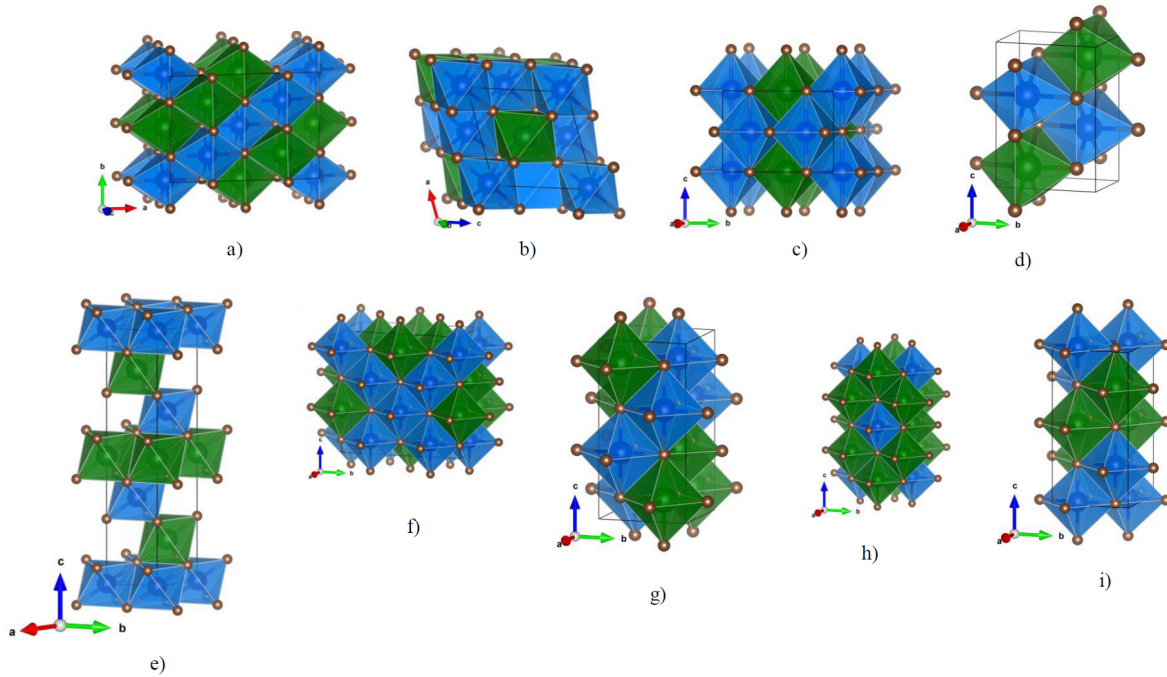


Figure 2. Crystal structures of $\text{Hf}_{0.5}\text{Ta}_{0.5}\text{C}$ structure candidates exhibiting the rock-salt structure proto-type: a) RS1, b) RS2, c) RS3, d) RS4, e) RS5, f) RS6, g) RS7, h) RS8 and i) RS9. Hf ions are shown as balls inside the green coordination polyhedra,

Ta ions are shown as balls inside the blue coordination polyhedra and the carbon atoms (brown balls) are located at the corners of the coordination polyhedral.

Table 1. Space group, unit cell parameters and atomic positions for the nine structure candidates in the $\text{Hf}_{0.5}\text{Ta}_{0.5}\text{C}$ system with the lowest energies as computed with LDA and PBE functionals (all nine structure candidates exhibit the rock-salt structure proto-type)

Structure candidates	LDA	PBE
RS1	<i>Cccm</i> (66) $a = 9.03 \text{ \AA}; b = 6.38 \text{ \AA}; c = 6.37 \text{ \AA}$ Ta1 0 0 3/4 Ta2 1/4 3/4 1/2 Hf1 0 1/2 3/4 Hf2 3/4 3/4 1/2 C1 0.0028 0.7568 1/2 C2 0.2465 0 3/4	<i>Cccm</i> (66) $a = 9.12 \text{ \AA}; b = 6.45 \text{ \AA}; c = 6.44 \text{ \AA}$ Ta1 0 0 3/4 Ta2 1/4 3/4 1/2 Hf1 1/2 0 3/4 Hf2 3/4 3/4 1/2 C1 0.0028 0.7566 1/2 C2 0.2465 0 3/4
RS2	<i>P2</i> (3) $a = 5.52 \text{ \AA}; b = 6.38 \text{ \AA}; c = 5.53 \text{ \AA}$ $\beta = 109.43^\circ$ Ta1 0 0.8289 0 Ta2 0 0.5802 1/2 Ta3 1/2 0.0786 0 Ta4 1/2 0.5815 0 Hf1 1/2 0.3301 1/2 Hf2 1/2 0.8289 1/2 Hf3 0 0.0787 1/2 Hf4 0 0.3302 0 C1 0.7532 0.5831 0.7535 C2 0.7502 0.0754 0.7576 C3 0.2530 0.3335 0.7537 C4 0.7497 0.8262 0.2445	<i>P2</i> (3) $a = 5.58 \text{ \AA}; b = 6.45 \text{ \AA}; c = 5.59 \text{ \AA}$ $\beta = 109.42^\circ$ Ta1 0 0.8288 0 Ta2 0 0.5805 1/2 Ta3 1/2 0.0783 0 Ta4 1/2 0.5802 0 Hf1 1/2 0.3302 1/2 Hf2 1/2 0.8288 1/2 Hf3 0 0.0787 1/2 Hf4 0 0.3303 0 C1 0.7531 0.5830 0.7534 C2 0.7502 0.0755 0.7575 C3 0.2529 0.3335 0.7535 C4 0.7497 0.8264 0.2447
RS3	<i>P4₂/mmc</i> (131) $a = 6.38 \text{ \AA}; c = 4.51 \text{ \AA}$ Ta 0 0.2490 1/2 Hf 1/2 0.2485 1/2 C1 0.2415 1/2 1/2 C2 0.7566 0 1/2	<i>P4₂/mmc</i> (131) $a = 6.45 \text{ \AA}; c = 4.56 \text{ \AA}$ Ta 0 0.7513 1/2 Hf 1/2 0.7517 1/2 C1 0.7583 1/2 1/2 C2 0.2437 0 1/2
RS4	<i>Pmnn</i> (59) $a = 3.18 \text{ \AA}; b = 4.52 \text{ \AA}; c = 6.39 \text{ \AA}$ Ta 3/4 1/4 0.6240 Hf 1/4 3/4 0.8735 C1 3/4 3/4 0.6186 C2 3/4 3/4 0.1338	<i>Pmnn</i> (59) $a = 3.22 \text{ \AA}; b = 4.56 \text{ \AA}; c = 6.46 \text{ \AA}$ Ta 3/4 1/4 0.6237 Hf 1/4 3/4 0.8732 C1 3/4 3/4 0.6189 C2 3/4 3/4 0.1337
RS5	<i>R-3m</i> (166) $a = 3.19 \text{ \AA}; c = 15.67 \text{ \AA}$ Ta 0 0 0 Hf 0 0 1/2 C 0 0 0.2534	<i>R-3m</i> (166) $a = 3.22 \text{ \AA}; c = 15.85 \text{ \AA}$ Ta 0 0 0 Hf 0 0 1/2 C 0 0 0.2533
RS6	<i>Amm2</i> (38) $a = 4.51 \text{ \AA}; b = 9.03 \text{ \AA}; c = 9.02 \text{ \AA}$ Ta1 0 0.2493 0.1083 Ta2 1/2 0 0.1081 Ta3 0 0 0.8589 Hf1 1/2 0 0.6087 Hf2 1/2 0.2491 0.8582 Hf3 0 0 0.3573 C1 0 0.2461 0.8584 C2 0 0 0.6121 C3 1/2 0.7535 0.1083 C4 1/2 0 0.3536 C5 1/2 0 0.8618 C6 0 0 0.1054	<i>Amm2</i> (38) $a = 4.56 \text{ \AA}; b = 9.12 \text{ \AA}; c = 9.11 \text{ \AA}$ Ta1 0 0.7509 0.8917 Ta2 1/2 0 0.8921 Ta3 0 0 0.1409 Hf1 1/2 0 0.3912 Hf2 1/2 0.7510 0.1418 Hf3 0 0 0.6427 C1 0 0.7539 0.1416 C2 0 0 0.3879 C3 1/2 0.2466 0.8917 C4 1/2 0 0.6464 C5 1/2 0 0.1383 C6 0 0 0.8944
RS7	<i>I4₁/amd</i> (141) $a = 4.51 \text{ \AA}; c = 9.03 \text{ \AA}$ Ta 1/2 3/4 7/8 Hf 0 3/4 1/8 C 0 3/4 0.3779	<i>I4₁/amd</i> (141) $a = 4.56 \text{ \AA}; c = 9.12 \text{ \AA}$ Ta 1/2 3/4 7/8 Hf 0 3/4 1/8 C 0 3/4 0.3778
RS8	<i>P4₂/mmc</i> (131) $a = 4.51 \text{ \AA}; c = 9.03 \text{ \AA}$ Ta1 1/2 0 0 Ta2 1/2 1/2 1/4 Hf1 1/2 0 1/2 Hf2 0 0 1/4 C1 1/2 1/2 0 C2 0 0 0 C3 0 1/2 0.2529	<i>P4₂/mmc</i> (131) $a = 4.55 \text{ \AA}; c = 9.13 \text{ \AA}$ Ta1 1/2 0 0 Ta2 1/2 1/2 1/4 Hf1 1/2 0 1/2 Hf2 0 0 1/4 C1 1/2 1/2 0 C2 0 0 0 C3 0 1/2 0.2529
RS9	<i>P4/nmm</i> (129) $a = 4.51 \text{ \AA}; c = 9.02 \text{ \AA}$ Ta1 1/4 1/4 0.7512 Ta2 3/4 1/4 0 Hf1 3/4 3/4 0.7509 Hf2 3/4 1/4 1/2 C1 3/4 3/4 0.0020 C2 3/4 3/4 0.4957 C3 1/4 3/4 0.2446	<i>P4/nmm</i> (129) $a = 4.56 \text{ \AA}; c = 9.12 \text{ \AA}$ Ta1 3/4 3/4 0.7517 Ta2 1/4 3/4 0 Hf1 1/4 1/4 0.7513 Hf2 1/4 3/4 1/2 C1 1/4 1/4 0.0019 C2 1/4 1/4 0.4957 C3 3/4 1/4 0.2447

2i) and two more orthorhombic ones, RS4 (Fig. 2d) and RS6 (Fig. 2f). The candidate with the highest symmetry is RS5 (Fig. 2e) adopting the trigonal $R\bar{3}m$ space group. This structure candidate has a typical polytypic alternation of layers with only hafnium in the octahedra followed by layers with only tantalum in the octahedra. Structure details including unit cell parameters and atomic positions for the RS1-RS9 structure candidates are given in Table 1.

Besides the candidates with the rock-salt structure type (RS1-RS9), the global search yielded only one low-energy candidate with a structure type different from the rock-salt type. It belongs to the nickel arsenide (NiAs) structure prototype and its ranking in comparison with the RS1 and RS9 structure candidates is given in Fig. 1c. According to the $E(V)$ curves, the $\text{Hf}_{0.5}\text{Ta}_{0.5}\text{C}$ with nickel arsenide structure prototype might be accessible in high-temperature conditions. Data of the relaxed unit cell parameters and atomic positions for the NiAs structure type candidate are given in Table 2 and the structure is shown in Fig. 3a. Since the NiAs prototype candidate appears in space group $Pmma$ (no. 51), it is distorted compared to the ideal (binary) nickel arsenide structure type that adopts the hexagonal $P6_3/mmc$ (no. 194) space group. Nevertheless, it shows the characteristic 6-fold coordination of the cations (hafnium and tantalum) by the anions (carbon) forming $ABAB$ layers of edge- and face-connected octahedra (Fig. 3a). Previous theoretical investigations have also found this structure type in a variety of AB systems [51–53].

In our previous studies, we have investigated HfC [29] and TaC [30], the end members of the $\text{Hf}_x\text{Ta}_{1-x}\text{C}$

system. The candidate ranked as the best in total energy for both end compounds adopts the rock-salt structure type, similar to the result we have obtained for the composition $x = 1/2$. The next two structure candidates, by energy, present in both end members exhibited two structure types called ortho-type and 5-5-type as number 2 and 3, respectively. Consequently, besides the structure candidates already obtained from the global search, we constructed the analogues for these two structure types in the $\text{Hf}_{0.5}\text{Ta}_{0.5}\text{C}$ system as candidates for low-energy structures.

The first one, originally denoted as ortho-type in ref. [29] since it adopts an orthorhombic symmetry, is depicted in (Fig. 3b) with structure parameters given in Table 2. Interestingly, the ortho-type structure candidate adopts the space group $Cmcm$ (no. 63) not only in pure HfC and TaC, but also for the $\text{Hf}_{0.5}\text{Ta}_{0.5}\text{C}$ system: for the energetically most favourable cation arrangement in the ortho-prototype, there was no reduction in symmetry compared to the pure system. This candidate in the new structure type, which is lower in total energy ranking than the nickel arsenide type candidate (Figs. 1c,d) can be visualized as a combination of the rock-salt and 5-5 types of structure, where the octahedra coordinating the Hf cations are edge-connected to the trigonal bipyramids coordinating the Ta cations (Fig. 3b) Very similar kinds of alternating combinations of octahedral and trigonal bipyramidal layers have been observed as local minima on the energy landscape of some ionic compounds, such as for bulk NaCl [54] or for monolayers of MgO on sapphire [23].

Table 2. Space group, unit cell parameters and atomic positions after local minimization using LDA and PBE functionals, for three additional relevant structure candidates in the $\text{Hf}_{0.5}\text{Ta}_{0.5}\text{C}$ system exhibiting the NiAs-, ortho- and 5-5-structure proto-types

Structure candidates	LDA	PBE
NiAs	$Pmma$ (51) $a = 5.53 \text{ \AA}; b = 3.17 \text{ \AA}; c = 5.51 \text{ \AA}$ Ta 0 1/2 1/2 Hf 0 0 0 C1 1/4 0 0.3446 C2 3/4 1/2 0.1811	$Pmma$ (51) $a = 5.58 \text{ \AA}; b = 3.21 \text{ \AA}; c = 5.58 \text{ \AA}$ Ta 0 1/2 1/2 Hf 0 0 0 C1 1/4 0 0.3439 C2 3/4 1/2 0.1809
Ortho	$Cmcm$ (63) $a = 3.33 \text{ \AA}; b = 13.30 \text{ \AA}; c = 4.47 \text{ \AA}$ Ta 0 0.9201 1/4 Hf 0 0.6869 1/4 C1 0 0.3199 1/4 C2 0 0.0753 1/4	$Cmcm$ (63) $a = 3.38 \text{ \AA}; b = 13.41 \text{ \AA}; c = 4.51 \text{ \AA}$ Ta 0 0.6862 1/4 Hf 0 0.9200 1/4 C1 0 0.3205 1/4 C2 0 0.0753 1/4
5-5	$P\bar{6}m2$ (187) $a = 3.72 \text{ \AA}; b = 4.47 \text{ \AA}$ Ta 2/3 1/3 0 Hf 1/3 2/3 1/2 C1 2/3 1/3 1/2 C2 1/3 2/3 0	$P\bar{6}m2$ (187) $a = 3.76 \text{ \AA}; b = 4.51 \text{ \AA}$ Ta 1/3 2/3 1/2 Hf 2/3 1/3 0 C1 2/3 1/3 1/2 C2 1/3 2/3 0

Besides the ortho-type structure, the so-called 5-5 structure had also been found during the global searches as a structure candidate in HfC and TaC, i.e.

in the end members of the hafnium tantalum composition range. Previously, this structure type has been found on the energy landscape of various AB

chemical systems [55,56] and experimentally for ZnO films [57] and NaCl monolayers [58]. According to Figs. 1c,d, the 5-5 type structure candidate can be expected to be thermodynamically stable in the negative pressure region at pressures below -30 GPa. The prototypical 5-5 structure type appears in the hexagonal symmetry with space group $P6_3/mmc$ (no. 194) in HfC and TaC, but for the $Hf_{0.5}Ta_{0.5}C$

composition, its symmetry is reduced to space group $P-6m2$ (no. 187) (Table 2). Nevertheless, the structural motif is preserved and can be described as a mutual fivefold coordination of cation A by anion B in a hexagonal lattice with $ABAB$ stacking, where the A-atoms form trigonal bipyramids around the B-atoms, and vice versa (Fig. 3c).

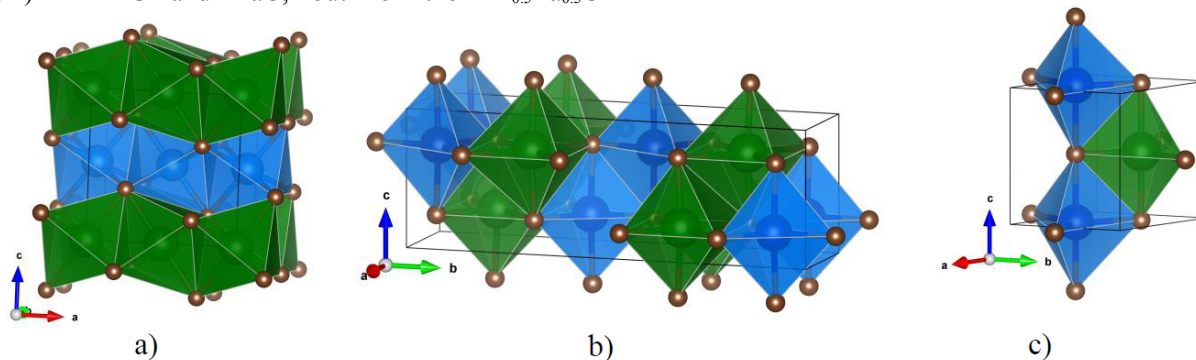


Figure 3. Crystal structure of $Hf_{0.5}Ta_{0.5}C$ structure candidates with structure type different from the rock-salt proto-type: a) NiAs structure proto-type; b) Ortho structure proto-type and c) 5-5 structure proto-type. Hf ions are shown as balls inside the green coordination polyhedra, Ta ions are shown as balls inside the blue coordination polyhedra and the carbon atoms are depicted as brown balls at the corners of the coordination polyhedra. Note that the octahedra in the ortho-type are filled by Hf ions and the trigonal bipyramids by Ta ions, respectively.

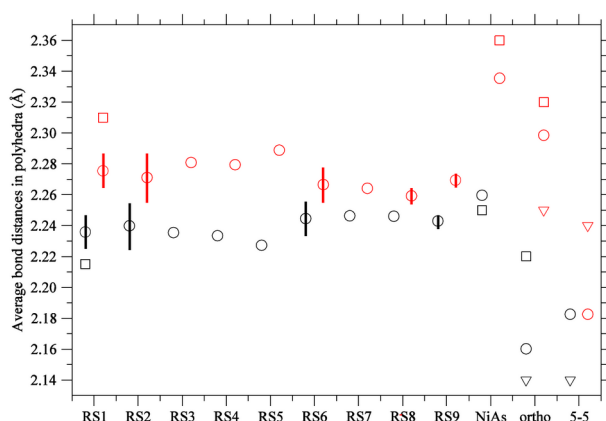


Figure 4. Average Hf-C and Ta-C bond distances in coordination polyhedra of the twelve most important $Hf_{0.5}Ta_{0.5}C$ structure candidates. Black circles and lines denote average distances and their spread in TaC_n coordination polyhedra ($n = 5,6$), and red circles and lines indicate the average distances and their spread in HfC_n polyhedra, respectively. Black (red) triangles and black (red) squares are given for comparison and denote the corresponding Ta-C (Hf-C) distances for trigonal bipyramidal and octahedral coordination polyhedra of the Ta (Hf) atoms, respectively, in the rock-salt, NiAs, ortho-, and 5-5 structure candidates for the pure compounds TaC and HfC. Note that in the ortho-type modification for the pure compounds TaC and HfC, half of the Ta and Hf atoms are six- and five-fold coordinated by C atoms.

We analysed the average values of cation-anion bond distances, and their spread, for the coordination polyhedra formed by the neighbouring carbon atoms around the Hf and Ta ions. For the candidates exhibiting the rock salt (RS1 - RS9) and the NiAs

structure prototypes, all these polyhedra are octahedra. For the 5-5 structure type, both cations are coordinated by five carbon atoms (Fig. 3c), and for the ortho-type one-half of the coordination polyhedra are trigonal bipyramids and the other half are octahedra. According to these results, the greatest spread in the atom distances occurs in the three structure candidates (RS1, RS2 and RS6), indicating the most pronounced octahedral distortion (Fig. 4). This also correlates with the observation that the space group symmetries of these three structure candidates are the lowest ones among the nine rock salt prototype structures.

Furthermore, considering the structures depicted in Fig. 2, the connectivity of the octahedra for these candidates appears to be such that the Hf- and Ta-centred octahedra are required to accommodate one another: thus the competition between forming ideal-size coordination octahedra around Hf and Ta, as found in the pure HfC and TaC compounds on one hand, and matching up with the slightly different octahedra surrounding the second cation, leads to stronger distortions. As a consequence, the Hf-C and Ta-C atom-atom nearest neighbour distances vary for the octahedra for a given central cation, but also are relatively similar when compared to the distances in the octahedra with the other central cations. This contrasts the structures where there is no distortion of the octahedra around Hf and Ta is observed: here, the difference between average bond distances for the HfC_6 and TaC_6 octahedra is more pronounced, while all the cation-carbon atom distances for a given cation, Hf or Ta, are nearly the same.

Regarding the NiAs prototype modification, the cation-carbon distances are nearly the same for the octahedra surrounding a given cation (Hf or Ta), but the difference between Ta–C and Hf–C atom-atom distances is the largest for all modifications analysed here. Considering the structure pictured in Fig. 3a, this is not such a surprise, since the NiAs prototype candidate structure is considerably distorted compared to the ideal NiAs type, thus allowing the alternating separate layers of TaC₆ and HfC₆ octahedra to form nearly identical - though systematically distorted (elongated or flattened) - coordination octahedra for each of the two cations, where all the Hf–C and Ta–C distances can be identical while the connecting edges and faces of these C₆-octahedra (of different diameter orthogonal to the *c*-axis) still match.

Regarding the ortho-type modification, the average cation-anion bond distance in the Hf-centred carbon octahedra is 2.30 Å, while in the trigonal bipyramids around tantalum, the Ta–C distances are 2.16 Å. In neither case, a noticeable spread in these distances is observed. This is no surprise since it is to be expected from classical ionic packings of anions around cations - or cations filling up holes in an anion packing - that the cation-anion distances are smaller for those coordination polyhedra with fewer numbers of surrounding anions.

Finally, we turn to the 5-5 proto-type structure candidate. Here, we observed no difference in the average bond distances regardless of whether the central cation is Hf or Ta. Furthermore, there is no spread in the anion-cation distances. This suggests that the spatial arrangement of the edge-connected trigonal carbon bipyramids is flexible enough to accommodate both cations in such a way that the carbon lattice does not need to get distorted when switching from a Hf to a Ta layer - in future work, it might be of interest to study the band gaps for these different modifications, to see whether the type and degree of distortions of the coordination carbon polyhedra can be related to differences in the electronic structure of the modification. Here, we also note that the average Ta–C atom distances inside the trigonal bipyramids for the ortho-type candidate are slightly smaller than the one for the 5-5 prototype structure; this is probably a reflection of the fact that the HfC₆ octahedra in the

ortho-type need to be accommodated and thus leads to a squeezing of the trigonal bipyramids, while in the 5-5 type the structure is more balanced. In the next step, we compared the average bond distances between the Hf_{0.5}Ta_{0.5}C system and the pure HfC and TaC compounds. This comparison is performed for the rock-salt, NiAs, ortho- and 5-5 structure candidates. In Fig. 4, squares and triangles denote average bond distances in octahedral and trigonal bipyramidal coordination, respectively, for Hf (red) and Ta (black) atoms by carbon atoms in the pure HfC and TaC compounds. We note that the cation-anion distances in the modifications of the pure compounds tend to be systematically larger (for Hf atoms) and shorter (for Ta atoms), respectively, than in the corresponding modifications of the mixed compound. This is somewhat expected since the original coordination polyhedra in the pure Hf(Ta) carbide must adjust towards some average value due to the presence of the other Ta(Hf) cation type in the neighbouring polyhedra. This is reminiscent of the Vegard's law for the size of the cell parameters in solid solution alloys as a function of composition, where an approximately linear interpolation of the cell parameters between the two end members of the composition range is found in the first order; on the atomic level, this adjustment results in slight enlargements and reductions of the coordination polyhedra in the smaller and larger end member compounds, respectively [59].

3.2. Mechanical and elastic properties of Hf_{0.5}Ta_{0.5}C

Since hafnium tantalum carbide is of great interest for practical applications due to its excellent mechanical properties, we have computed various (mesoscopic) mechanical and elastic properties, such as the bulk and shear modulus, the Vickers hardness, and the elastic constants C_{ij} . Since our calculations suggest that the rock salt prototype modification of Hf_{0.5}Ta_{0.5}C should be realized as a solid solution phase, in agreement with the experiment, the KOVIN algorithm [43] was employed to compute the mechanical and elastic properties for the case of a solid solution in the rock salt prototype, such that the cubic *Fm-3m* space group symmetry of this prototype could be preserved during the calculations.

Table 3. Comparison of the computed bulk (K_H), shear (G_H) and Young's modulus (E_{-H}), Poisson ratio (ν_{-H}), Vickers hardness (V_H) and elastic tensor constants, using the LDA functional for the solid solution case, with previous experimental and theoretical results in Hf_{0.5}Ta_{0.5}C

Hf _{0.5} Ta _{0.5} C	K_H [GPa]	G_H [GPa]	E_{-H} [GPa]	ν_{-H}	V_H [GPa]	Elastic tensor constants [GPa]
This study	325.30	228.88	556.19	0.215	28.89	$C_{11} = 717$; $C_{12} = 130$; $C_{44} = 194$
Theory [61]	276.4	194.1	471.8	0.22	25.84	$C_{11} = 614.6$; $C_{12} = 107.2$; $C_{44} = 162.1$
Theory [20]	282	210	504	-	29	$C_{11} = 627.2$; $C_{12} = 108.9$; $C_{44} = 182.5$

Exp.	298 [13]	212.28 [13]	523.82 [6]; 412 [61]	0.22 [61]	21.16 [61]	$C_{11} = 654; C_{12} = 120;$ $C_{44} = 182$
------	----------	-------------	-------------------------	-----------	------------	---

3.2.1. Bulk modulus, shear modulus, Young's modulus and Vickers hardness

Using the KOVIN algorithm [50], the values of the bulk, shear and Young's moduli, the elastic constants and the Vickers hardness were computed for a solid solution of $Hf_{0.5}Ta_{0.5}C$ composition in the rock salt type structure. These results are presented in Table 3, and a comparison with previous experimental and theoretical results, where available, shows a good agreement of our results with the reported data.

Besides the calculations that approximated the experimentally observed solid solution, we also computed the above-mentioned mechanical and elastic parameters for the nine individual structure candidates with the lowest energy, which had been obtained during the global search in the $Hf_{0.5}Ta_{0.5}C$ system and exhibited the rock salt prototype structure. From Figs. 5a-d depicting the four properties, bulk, shear, Young modulus and the Vickers hardness, we can conclude that the values are quite uniform and barely change

among the nine structure candidates. For example, the bulk modulus values lie between 325.01 GPa (RS4) and 328.90 (RS8) - a spread of 1% -, and the shear modulus varies between 233.14 GPa (RS3) and 238.26 (RS5) GPa - a spread of 2% -, while the corresponding values computed for the solid solution are 325.30 GPa and 228.88 GPa, respectively. The lowest Vickers hardness is found again for the RS3 candidate (29.91 GPa), while the candidate with the highest Vickers hardness is RS5 (31.28 GPa) - a spread of 4% -, and for the solid solution we obtain 28.89 GPa. The spread in the values for Young's modulus between the lowest value 564.48 GPa (RS3) and the highest value 579.63 GPa (RS8) is also quite small (about 2.5%), where the value for the solid solution is 556.19 GPa. The complete list of mechanical parameters can be found in the Supplementary material (Table S2), where besides the results obtained using the LDA functional we present also the ones for the GGA functional.

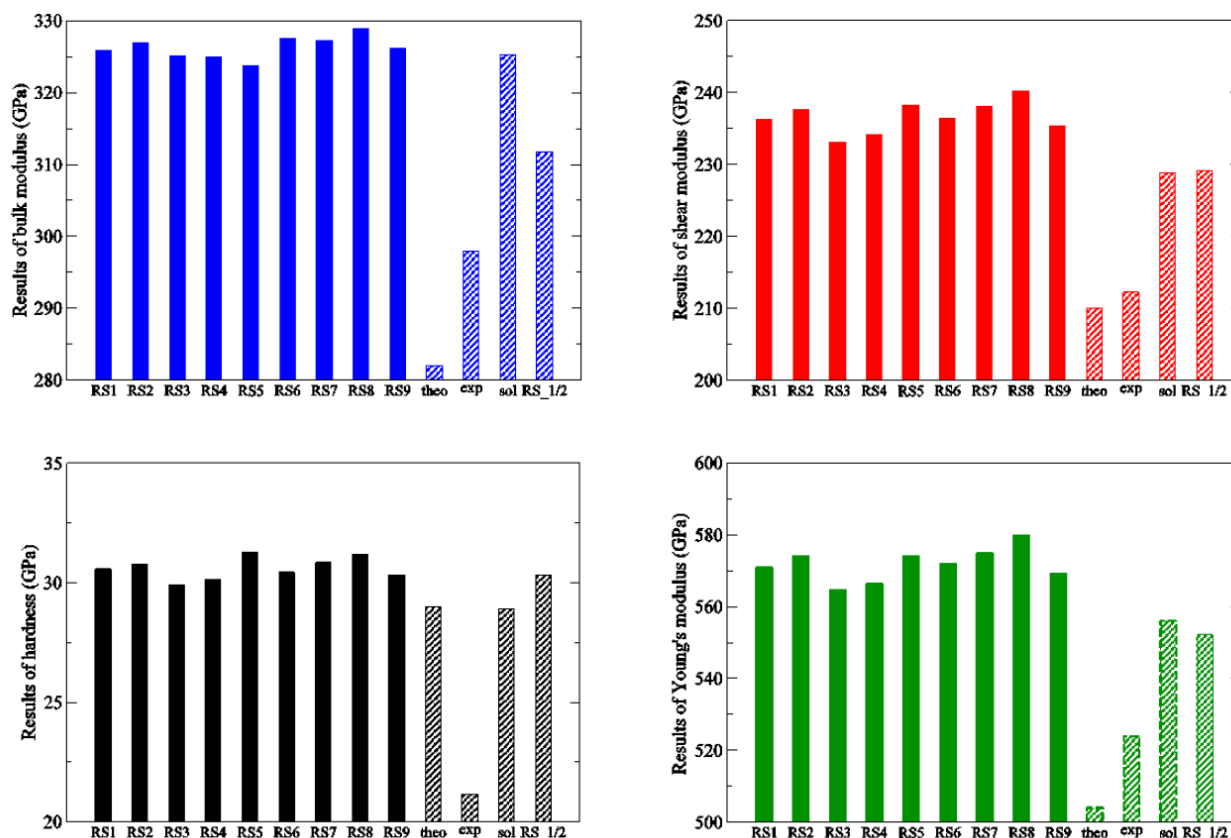


Figure 5. Results of: a) bulk modulus, b) shear modulus, c) hardness and d) Young's modulus for the nine $Hf_{0.5}Ta_{0.5}C$ candidates with the lowest energies and available theoretical (theo) [6] and experimental (exp) [20] results from the literature (c.f. Table 3), whose structures belong to the rock salt proto-type, obtained using the LDA functional. We also include the values for our solid solution calculations (sol) from Table 3, and the average values for the pure compounds, "1/2(HfC+TaC)", (RS 1/2), for comparison

It is interesting to compare the values of the mechanical parameters obtained for the case of the

cubic solid solution structure with the full $Fm-3m$ symmetry (Table 3) with the results for the individual

rock salt prototype structure candidates, which exhibit lower symmetries (Fig. 5). We observe that the individual rock salt prototype candidates have on average slightly higher values than the solid solution for all four properties. However, the values of the Young modulus and the bulk modulus obtained for the solid solution are within the spread, and the values of the shear modulus and the Vickers hardness for the solid solution are only about 3% smaller than the average values for the set of the nine rock salt prototype minimum structures. This small spread in the values serves as a further support that in the $\text{Hf}_{0.5}\text{Ta}_{0.5}\text{C}$ system, the thermodynamically stable phase should be a solid solution phase, in agreement with experiments. Finally, the comparison between the

averages for the computed values for the pure compounds and the ones computed for the RS1 modification (c.f. Table S4 in the SI), shows that the average values of the two pure compounds tend to be slightly lower than the value for the mixed compound (ca. 3–4%) and are quite similar to or slightly smaller than the values obtained from the solid solution calculations of the properties for the mixed compound. This suggests that $\text{Hf}_{0.5}\text{Ta}_{0.5}\text{C}$ should exhibit similar or even better properties compared to a granular (sintered) mixture of HfC and TaC without the stability problems (e.g. the presence of cavities, weak interfaces between HfC and TaC crystallites, etc.) associated with such a granular type material.

Table 4. Elastic constants in GPa for those $\text{Hf}_{0.5}\text{Ta}_{0.5}\text{C}$ structure candidates belonging to the rock salt structure type, obtained using the LDA functional

RS1	RS 2	RS3	RS4	RS5	RS6	RS7	RS8	RS9
	$C_{11} = 633$							
	$C_{12} = 156$							
$C_{11} = 732$	$C_{13} = 195$		$C_{11} = 635$		$C_{11} = 734$			
$C_{12} = 123$	$C_{15} = -49$		$C_{12} = 120$		$C_{12} = 124$			
$C_{13} = 121$	$C_{22} = 632$	$C_{11} = 625$	$C_{13} = 231$	$C_{11} = 630$	$C_{13} = 125$	$C_{11} = 736$	$C_{11} = 739$	$C_{11} = 732$
$C_{22} = 628$	$C_{23} = 190$	$C_{12} = 226$	$C_{22} = 728$	$C_{12} = 162$	$C_{22} = 724$	$C_{12} = 123$	$C_{12} = 126$	$C_{12} = 122$
$C_{23} = 226$	$C_{25} = 45$	$C_{13} = 125$	$C_{23} = 123$	$C_{13} = 187$	$C_{23} = 130$	$C_{13} = 124$	$C_{13} = 125$	$C_{13} = 125$
$C_{33} = 634$	$C_{33} = 594$	$C_{33} = 725$	$C_{33} = 614$	$C_{14} = 0$	$C_{33} = 731$	$C_{33} = 730$	$C_{33} = 730$	$C_{33} = 728$
$C_{44} = 299$	$C_{35} = 2$	$C_{44} = 196$	$C_{44} = 200$	$C_{33} = 588$	$C_{44} = 201$	$C_{44} = 199$	$C_{44} = 204$	$C_{44} = 199$
$C_{55} = 198$	$C_{44} = 265$	$C_{66} = 297$	$C_{55} = 300$	$C_{44} = 271$	$C_{55} = 202$	$C_{66} = 206$	$C_{66} = 207$	$C_{66} = 197$
$C_{66} = 200$	$C_{46} = 46$		$C_{66} = 195$		$C_{66} = 199$			
	$C_{55} = 273$							
	$C_{66} = 234$							

3.2.2 Elastic constants

The elastic constants for the nine structure candidates that exhibit the rock salt prototype structure are given in Table 4. Since these candidates belong to different crystal systems, including monoclinic (RS2), orthorhombic (RS1, RS4, RS6), tetragonal (RS3, RS7, RS8, RS9) and rhombohedral (RS5) ones, a different set of elastic constants had to be computed for each crystal system. Furthermore, since the strain energy has to be positive, in order to ensure mechanical stability, based on the Born-Huang criteria [47], the Born stability conditions or sufficient elastic stability criteria were calculated for each candidate.

According to the elastic constants presented in Table 4 and the calculated mechanical stability conditions, it is clear that stability criteria are satisfied for the candidates belonging to the tetragonal, orthorhombic, and rhombohedral crystal systems, suggesting that all these structure candidates are mechanically stable.

Regarding the monoclinic RS2 modification, we note the presence of a negative elastic constant, C_{15} . However, in previous investigations in the literature [60], the possible reason for this appearance of a negative elastic constant in some structures in the monoclinic crystal system has been discussed in detail:

Since the a axis in the monoclinic system is inclined against the x_1 axis, the shear strain in the x_1 - x_3 plane caused by tensile stress along the x_1 axis decreases the angle between the x_1 axis and the a axis, i.e. the shear angle. As a result, C_{15} can become negative, even though the structure itself is mechanically stable. This applies in our case, since during the calculations of the elastic constants, the three orthogonal principal axes employed for computations in the monoclinic system (x_1 , x_2 and x_3) were defined as follows in the *ab initio* code: the x_2 and x_3 axes are along the b and c axes, respectively, and the x_1 axis is taken to be perpendicular to the x_2 - x_3 plane; due to the monoclinic space group of RS2, the x_1 axis is not parallel to the a axis because the angle between the a and c axes is not 90° but 109.43° for RS2.

3.3.3 Elastic and mechanical properties

Furthermore, the same kind of analysis was performed for other three promising structure candidates, which exhibited the distorted NiAs structure prototype and the ortho- and 5-5 structure prototypes. Table S3 in the Supplementary Material presents the computed values for the bulk modulus, shear modulus, Young's modulus, Vickers hardness and the elastic constants. Here, the results obtained

using LDA and GGA-PBE functionals are both listed. Overall, the values of the bulk, shear and Young's modulus, and of the Vickers hardness for the NiAs prototype modification are about 10–20% lower than for the candidates with rock salt structure type, and the corresponding values for the ortho- and 5-5-prototype modifications are even smaller, exhibiting also a much greater spread in the different schemes employed to compute the mechanical properties, e.g. the Vickers hardness varies between 0.09 and 10.99 GPa for the 5-5 prototype structure. Regarding the mechanical stability computed from the elastic parameters, both the 5-5 prototype and the NiAs prototype modifications would be stable, but the stability of the ortho prototype structure candidate is doubtful since we obtained negative values for C_{66} with both functionals. Again, the average of these values for the two compounds HfC and TaC are quite similar to those determined for the mixed compound $\text{Hf}_{0.5}\text{Ta}_{0.5}\text{C}$ (c.f., Table S4).

IV. Conclusions

We have determined possible crystal structure candidates in the $\text{Hf}_{0.5}\text{Ta}_{0.5}\text{C}$ system via global optimizations for different pressures using empirical potentials. The crystal structures found on the energy landscape were further locally optimized on the *ab initio* level. The rock salt prototype structure is found as a global minimum in agreement with experimental data, and the nine structures with the lowest energy all represent distorted versions of the rock-salt prototype (denoted as RS1-RS9). In addition, the search for low-energy minima yielded a promising structure candidate exhibiting a nickel-arsenide prototype structure, and two additional structure candidates were constructed based on previously found low-energy candidates in the pure HfC and TaC systems, belonging to the so-called ortho and 5-5 structure prototypes.

The analysis of the energies, $E(V)$ curves, and mechanical and elastic properties showed that the thermodynamically stable phase of $\text{Hf}_{0.5}\text{Ta}_{0.5}\text{C}$ should be a solid solution exhibiting the rock salt structure prototype, down to moderate temperatures, in agreement with the experiment. At high temperatures, the NiAs structure candidate might be accessible as a metastable modification, while in the effective negative pressure region the 5-5 prototype structure would be thermodynamically stable. Thus, this 5-5 prototype structure might be accessible as an alternative stable modification, e.g. via growth from an amorphous low-density film deposited from the gas phase. Furthermore, our calculations of the elastic constants and mechanical properties, on the *ab initio* level, are in good agreement with the previous experimental and theoretical data. The variation of the mechanical and elastic properties among the different

rock salt prototype structures contributing to the solid solution state, was very small, which indicates that the solid solution phase should be quite stable even under high-pressure applications. These results provide new insights into the thermodynamic, mechanical and elastic properties of the $\text{Hf}_{0.5}\text{Ta}_{0.5}\text{C}$ system, both regarding the experimentally known solid solution phase and the existence of possible alternative modifications.

Acknowledgments: This research was funded by the Ministry of Science, Technological Development and Innovation of the Republic of Serbia through Contract Nos. 451-03-66/2024-03/200017 and 451-03-136/2025-03/200017. The authors are grateful to R. Dovesi, K. Doll, and Crystal Solutions for software support with CRYSTAL code.

References

- O. Cedillos-Barraza, S. Grasso, N.A. Nasiri, D.D. Jayaseelan, M.J. Reece, W.E. Lee, "Sintering behaviour, solid solution formation and characterisation of TaC, HfC and TaC–HfC fabricated by spark plasma sintering", *J. Eur. Ceram. Soc.*, **36** (2016) 1539–1548.
- L. Silvestroni, L. Pienti, S. Guicciardi, D. Sciti, "Strength and toughness: The challenging case of TaC-based composites", *Composites Part B: Eng.*, **72** (2015) 10–20.
- A.A. Lavrentyev, B.V. Gabrelian, V.B. Vorzhev, I.Y. Nikiforov, O.Y. Khyzhun, J.J. Rehr, "Electronic structure of cubic $\text{Hf}_x\text{Ta}_{1-x}\text{C}_y$ carbides from X-ray spectroscopy studies and cluster self-consistent calculations", *J. Alloys Compd.*, **462** (2008) 4–10.
- J. Li, X. Wang, K. Liu, D. Li, L. Chen, "Crystal structures, mechanical and electronic properties of tantalum monocarbide and mononitride", *J. Superhard Mater.*, **33** (2011) 173–178.
- S.A. Ghaffari, M.A. Faghihi-Sani, F. Golestani-Fard, M. Nojabayy, "Diffusion and solid solution formation between the binary carbides of TaC, HfC and ZrC", *Int. J. Refractory Met. Hard Mater.*, **41** (2013) 180–184.
- C. Zhang, A. Gupta, S. Seal, B. Boesl, A. Agarwal, "Solid solution synthesis of tantalum carbide-hafnium carbide by spark plasma sintering", *J. Am. Ceram. Soc.*, **100** (2017) 1853–1862.
- C. Zhang, A. Loganathan, B. Boesl, A. Agarwal, "Thermal analysis of tantalum carbide-hafnium carbide solid solutions from room temperature to 1400 °C", *Coatings*, **7** (2017) 111.
- R. Shannon, "Revised effective ionic radii and systematic studies of interatomic distances in halides and chalcogenides", *Acta Crystal. A*, **32** (1976) 751–767.
- C. Agte, H. Alterthum, "Systems of high-melting carbides: Contributions to the problem carbon fusion", *Technic. Phys.*, **11** (1930) 182–191.
- O. Cedillos-Barraza, S. Grasso, N. Al Nasiri, D.D. Jayaseelan, M.J. Reece, W.E. Lee, "Sintering behaviour, solid solution formation and characterisation of TaC,

- HfC and TaC-HfC fabricated by spark plasma sintering”, *J. Eur. Ceram. Soc.*, **36** (2016) 1539–1548.
11. D. Rowcliffe, G. Hollox, “Plastic flow and fracture of tantalum carbide and hafnium carbide at low temperatures”, *J. Mater. Sci.*, **6** (1971) 1261–1269.
 12. H. Yu, M. Bahadori, G.B. Thompson, C.R. Weinberger, “Understanding dislocation slip in stoichiometric rocksalt transition metal carbides and nitrides”, *J. Mater. Sci.*, **52** (2017) 6235–6248.
 13. C.J. Smith, X.-X. Yu, Q. Guo, C.R. Weinberger, G.B. Thompson, “Phase, hardness, and deformation slip behavior in mixed $\text{Hf}_x\text{Ta}_{1-x}\text{C}$ ”, *Acta Mater.*, **145** (2018) 142–153.
 14. P. Froughi, C. Zhang, A. Agarwal, Z. Cheng, “Controlling phase separation of TaHf1-C solid solution nanopowders during carbothermal reduction synthesis”, *J. Am. Ceram. Soc.*, **100** (2017) 5056–5065.
 15. J. Zhang, S. Wang, W. Li, Y. Yu, J. Jiang, “Understanding the oxidation behavior of Ta–Hf–C ternary ceramics at high temperature”, *Corrosion Sci.*, **164** (2020) 108348.
 16. J. Zhang, S. Wang, W. Li, “Consolidation and characterization of highly dense single-phase Ta–Hf–C solid solution ceramics”, *J. Am. Ceram. Soc.*, **102** (2019) 58–62.
 17. H. Chen, Y. Zhang, Y. Fu, J. Meng, Q. Miao, J. Zhang, H. Li, “ $(\text{Hf}_{0.5}\text{Ta}_{0.5})\text{C}$ ultra-high temperature ceramic solid solution nanowires”, *J. Mater. Sci. Technol.*, **147** (2023) 91–101.
 18. G. Mu, Y. Liu, X. Tian, Z. Ma, S. Zhu, L. Liu, S. He, H. Chi, “First-principles calculation, synthesis, and oxidation mechanism of $\text{Ta}_{1-x}\text{Hf}_x\text{C}$ ultra-high temperature ceramics”, *Int. J. Refractory Met. Hard Mater.*, **123** (2024) 106744.
 19. T. Thomas, A. Nisar, C. Zhang, S. Joglekar, M. Pankow, B. Boesl, A. Agarwal, “High strain rate response and mechanical performance of tantalum carbide–hafnium carbide solid solution”, *Ceram. Int.*, **49** (2023) 39099–39106.
 20. W.U. Yuhao, P. Renci, C. Chunyu, Y. Li, Z. Yichun, “First-principles study on mechanical properties and melting curve of $\text{Hf}_x\text{Ta}_{1-x}\text{C}$ system”, *J. Inorg. Mater.*, **39** (2024) 761–768.
 21. D. Yu, J. Yin, B. Zhang, X. Liu, Z. Huang, “Recent development of high-entropy transitional carbides: a review”, *J. Ceram. Soc. Jpn.*, **128** (2020) 329–335.
 22. J.C. Schön, “Energy landscapes in inorganic chemistry”, pp. 262–392 in *Comprehensive Inorganic Chemistry III* (Third Edition), Eds. J. Reedijk, K.R. Poepelmeier, Elsevier, Oxford, 2023.
 23. J.C. Schön, “Nanomaterials - What energy landscapes can tell us”, *Process. Appl. Ceram.*, **9** (2015) 157–168.
 24. Ž.P. Čančarević, J.C. Schön, M. Jansen, “Structure prediction of solids: Heuristic algorithms for local optimization on Hartree-Fock level”, *Mater. Sci. Forum*, **453-454** (2004) 71–76.
 25. R. Hundt, J.C. Schon, A. Hannemann, M. Jansen, “Determination of symmetries and idealized cell parameters for simulated structures”, *J. Appl. Crystal.*, **32** (1999) 413–416.
 26. A. Hannemann, R. Hundt, J.C. Schön, M. Jansen, “A new algorithm for space-group determination”, *J. Appl. Crystal.*, **31** (1998) 922–928.
 27. R. Hundt, *KPLOT, A Program for Plotting and Analyzing Crystal Structures*, Technicum Scientific Publishing, Stuttgart, Germany, 2016.
 28. R. Hundt, J.C. Schön, M. Jansen, “CMPZ– an algorithm for the efficient comparison of periodic structures”, *J. Appl. Crystal.*, **39** (2006) 6–16.
 29. J. Zagorac, J.C. Schön, B. Matović, S. Butulija, D. Zagorac, “Hafnium carbide: Prediction of crystalline structures and investigation of mechanical properties”, *Crystals*, **14** (2024) 340.
 30. D. Zagorac, J. Zagorac, T. Škundrić, M. Pejić, D. Jovanović, J.C. Schön, “Structure prediction and mechanical properties of tantalum carbide (TaC) on ab initio level”, *Z. Anorg. Allg. Chem.*, **650** (2024) e202400088.
 31. K. Momma, F. Izumi, “VESTA: a three-dimensional visualization system for electronic and structural analysis”, *J. Appl. Crystal.*, **41** (2008) 653–658.
 32. R. Dovesi, A. Erba, R. Orlando, C.M. Zicovich-Wilson, B. Civalleri, L. Maschio, M. Rérat, S. Casassa, J. Baima, S. Salustro, B. Kirtman, “Quantum-mechanical condensed matter simulations with CRYSTAL”, *WIREs Comput. Mol. Sci.*, **8** (2018) e1360.
 33. R. Dovesi, F. Pascale, B. Civalleri, K. Doll, N.M. Harrison, I. Bush, P. D’Arco, Y. Noël, M. Rérat, P. Carbonnière, M. Causà, S. Salustro, V. Lacivita, B. Kirtman, A.M. Ferrari, F.S. Gentile, J. Baima, M. Ferrero, R. Demichelis, M. De La Pierre, “The CRYSTAL code, 1976–2020 and beyond, a long story”, *J. Chem. Phys.*, **152** (2020) 204111.
 34. J.P. Perdew, A. Zunger, “Self-interaction correction to density-functional approximations for many-electron systems”, *Phys. Rev. B*, **23** (1981) 5048–5079.
 35. J.P. Perdew, K. Burke, M. Ernzerhof, “Generalized gradient approximation made simple”, *Phys. Rev. Lett.*, **77** (1996) 3865–3868.
 36. A. Grzechnik, B.V. Hakala, S. Kurig, N. Walte, N. Tsujino, S. Kakizawa, Y. Higo, D. Zagorac, J. Zagorac, R. Dronskowski, J.C. Schön, K. Friese, “Structures, phase stability, amorphization, and decomposition of V_6O_{13} at high pressures and temperatures: Synthesis of rutile-related $\text{V}_{0.92}\text{O}_2$ ”, *Crystal Growth Design*, **24** (2024) 5582–5592.
 37. D. Muñoz Ramo, J.L. Gavartin, A.L. Shluger, G. Bersuker, “Spectroscopic properties of oxygen vacancies in monoclinic HfO_2 calculated with periodic and embedded cluster density functional theory”, *Phys. Rev. B*, **75** (2007) 205336.
 38. D. Zagorac, M. Fonović, S. Butulija, A. Luković, V. Maksimović, J. Zagorac, B. Matović, “A multi-disciplinary study of yttrium effect on the electronic structure of hafnia”, *J. Alloys Compd.*, **1010** (2025) 178343.
 39. G. Sophia, P. Baranek, C. Sarrazin, M. Rérat, R. Dovesi, “First-principles study of the mechanisms of the pressure-induced dielectric anomalies in ferroelectric perovskites”, *Phase Transit.*, **86** (2013) 1069–1084.
 40. D.T. Teppala, J. Bernauer, A. Rashid, M. Pejić, D. Zagorac, B. Matovic, E. Ionescu, “Single-source precursor synthesis of a compositionally complex early

- transitional metal carbonitride (Ti,Zr,Hf,Nb,Ta)NC1”, *Adv. Eng. Mater.*, **26** (2024) 2302165.
41. M. Catti, A. Pavese, R. Dovesi, V.R. Saunders, “Static lattice and electron properties of MgCO₃ (magnesite) calculated by ab initio periodic Hartree-Fock methods”, *Phys. Rev. B, Condensed Matter*, **47** (1993) 9189–9198.
 42. R. Hill, “The elastic behaviour of a crystalline aggregate”, *Proceed. Physical Society, Section A*, **65** (1952) 349–354.
 43. Y. Tian, B. Xu, Z. Zhao, “Microscopic theory of hardness and design of novel *superhard crystals*”, *Int. J. Refractory Met. Hard Mater.*, **33** (2012) 93–106.
 44. M. Born, K. Huang, *Dynamical Theory of Crystal Lattices*, Clarendon Press, 1988.
 45. F. Mouhat, F.-X. Coudert, “Necessary and sufficient elastic stability conditions in various crystal systems”, *Phys. Rev. B*, **90** (2014) 224104.
 46. R.A. Cowley, “Acoustic phonon instabilities and structural phase transitions”, *Phys. Rev. B*, **13** (1976) 4877–4885.
 47. A. Gusev, S. Sadovnikov, “Conditions of elastic mechanical stability and elastic properties of crystal structures with different symmetry”, *Phys. Solid State*, **64** (2022) 659.
 48. W.F. Perger, J. Criswell, B. Civalleri, R. Dovesi, “Ab-initio calculation of elastic constants of crystalline systems with the CRYSTAL code”, *Computer Phys. Commun.*, **180** (2009) 1753–1759.
 49. A. Erba, A. Mahmoud, R. Orlando, R. Dovesi, “Elastic properties of six silicate garnet end members from accurate ab initio simulations”, *Phys. Chem. Minerals*, **41** (2014) 151–160.
 50. D. Zagorac, C. Buyer, J. Zagorac, T. Škundrić, J.C. Schön, T. Schleid, “Band-gap engineering and unusual behavior of electronic properties during anion substitution of sulfur in LaFSe”, *Crystal Growth Design*, **24** (2024) 1648–1657.
 51. Ž.P. Čančarević, J.C. Schön, M. Jansen, “Stability of alkali metal halide polymorphs as a function of pressure”, *Chem. Asian J.*, **3** (2008) 561–572.
 52. D. Zagorac, J.C. Schön, J. Zagorac, M. Jansen, “Prediction of structure candidates for zinc oxide as a function of pressure and investigation of their electronic properties”, *Phys. Rev. B*, **89** (2014) 075201.
 53. D. Zagorac, K. Doll, J.C. Schön, M. Jansen, “Ab initio structure prediction for lead sulfide at standard and elevated pressures”, *Phys. Rev. B*, **84** (2011) 045206.
 54. J.C. Schön, M. Jansen, “Determination of candidate structures for simple ionic compounds through cell optimisation”, *Comput. Mater. Sci.*, **4** (1995) 43–58.
 55. J.C. Schön, „Enthalpy landscapes of the earth alkaline metal oxides“, *Z. Anorg. Allg. Chem.*, **630** (2004) 2354–2366.
 56. D. Zagorac, J.C. Schön, M. Jansen, “Identification of promising chemical systems for the synthesis of new materials structure types: An ab initio minimization data mining approach”, *Process. Appl. Ceram.*, **7** (2013) 37–41.
 57. C. Tusche, H.L. Meyerheim, J. Kirschner, “Observation of depolarized ZnO(0001) monolayers: Formation of unreconstructed planar sheets”, *Phys. Rev. Lett.*, **99** (2007) 026102.
 58. K.A. Tikhomirova, C. Tantardini, E.V. Sukhanova, Z.I. Popov, S.A. Evlashin, M.A. Tarkhov, V.L. Zhdanov, A.A. Dudin, A.R. Oganov, D.G. Kvashnin, A.G. Kvashnin, “Exotic two-dimensional structure: The first case of hexagonal NaCl”, *J. Phys. Chem. Lett.*, **11** (2020) 3821–3827.
 59. L. Vegard, “Die Konstitution der Mischkristalle und die Raumfüllung der Atome”, *Zeitschrift für Physik*, **5** (1921) 17–26.
 60. K. Adachi, H. Ogi, N. Takeuchi, N. Nakamura, H. Watanabe, T. Ito, Y. Ozaki, “Unusual elasticity of monoclinic β-Ga₂O₃”, *J. Appl. Phys.*, **124** (2018) 085102.
 61. Y.-t. Zhang, S.-M. Li, N. Li, K. Li, X.-H. Shi, H.-J. Li, “Experimental and theoretical study on electronic structure and mechanical property of Ta_xHf_{1-x}C”, *J. Alloys Compd.*, **884** (2021) 161040.